

Ultra-Brilliant Twisted GeV Gamma-ray beam in QED Regime

Zheng Gong¹, Ronghao Hu¹, Haiyang Lu¹, Jinqing Yu¹, Chia-erh Chen¹, Xiantu He¹, and Xueqing Yan^{1,2,*}

¹State Key Laboratory of Nuclear Physics and Technology, and Key Laboratory of HEDP of the Ministry of Education, CAPT, Peking University, Beijing, China, 100871

²Collaborative Innovation Center of Extreme Optics, Shanxi University, Taiyuan, Shanxi, China, 030006

*x.yan@pku.edu.cn

ABSTRACT

The ability of rotating black holes to imprint orbital angular momentum (OAM) on the cosmic rays indicates that measuring the OAM spectra of cosmological gamma ray bursts is a promising route to detect the existence of black holes in the universe. An alternative method of generating violent emission of gamma rays is utilizing the interaction of petawatt (10^{15} W) lasers and plasmas in the laboratory, whereas none of the previous investigation involves the realization of twisted gamma rays up to GeV. Here we present an all-optical scheme for studying a laser-plasma based incoherent photon emission with an intrinsic OAM in quantum electrodynamic (QED) regime. A theoretical model is also proposed to explain the dynamic properties of OAM and energy transformation from electromagnetic fields to particles. 3D Particle-in-cell (PIC) simulations manifest our twisted gamma-ray flash with an unprecedented power of multi-petawatt (PW) and brightness of 1.7×10^{23} photons/s/mm²/mrad²/0.1% bandwidth (at 1 GeV) taking advantage of a prospective $\sim 10^{23}$ W/cm² scale laser facility. These results bode well for new research direction in particle physics and laboratory astrophysics while exploring laser plasma interaction.

Introduction

The twisted light with OAM is a beam possessing helical phase fronts, characterized by an azimuthal phase dependence¹. An additional degree of freedom makes the twisted light sources unique and potentially advantageous for applications in a wide range of fields, such as micromanipulation², optical data transmission^{3,4} and quantum information^{5,6}. Meanwhile, a series of proposed schemes⁷⁻⁹ paved the way to produce the twisted light from radiowave to ultraviolet spectrum in the past few decades. Recently, both spiral electron beams in helical undulator^{10,11} and inverse backscattering with Laguerre-gaussian beam¹² have realized a x-ray with OAM in keV range to investigate matter at attosecond time and angstrom length scales. Moreover, the previously inaccessible twisted gamma-ray from tens of MeV to GeV range is of key significance for studying the contribution of quark/gluon OAM to proton spin¹³ in elementary particle physics and the gamma burst OAM spectra¹⁴ imprinted by the rotating black holes¹⁵ in the astrophysics.

On the other hand, several multi-PW laser facilities, such as Extreme Light Infrastructure (ELI)¹⁶ and Exawatt Center for Extreme Light Studies (XCELS)¹⁷, are expected to operate at intensities beyond 10^{23} W/cm² in next few years. The rapid development of laser technology has unlocked new areas of laser plasma interaction in radiation dominant regime^{18,19} and exotic QED regime^{20,21}. At laser intensity $\sim 10^{23}$ W/cm², various theoretical schemes²²⁻²⁵ have been put forward for multi-MeV photon sources with tens of percent for the total conversion efficiency through synchrotron-like radiation, nevertheless, none of them possesses a well-defined OAM state like the helical phase front. Here we propose an all-optical scheme for an ultra-brilliant twisted GeV gamma-ray emission via irradiating a non-rotating circularly polarized (CP) laser pulse on a compound target in QED regime.

Theoretical model

In the realm of nonlinear QED, electrons are able to emit a huge amount of kinetic energy in the form of high-energy γ_{ph} photons, as a result of absorbing a certain number n of laser photons γ_l , $e^- + n\gamma_l \rightarrow e^- + \gamma_{ph}$. $\eta \simeq \gamma|\mathbf{E}_\perp + \mathbf{v} \times \mathbf{B}|/E_{Sch}$ is the ratio of electric field in the electron rest frame to $E_{Sch} = m_e^2 c^3 / e\hbar$, the characteristic field of Schwinger limit²⁶, where m_e is the electron rest mass and c is the light velocity in vacuum. When an electron beam co-propagates with the laser pulse, it results in $\eta \simeq 0$, which is undesired for high-energy photon emission^{19,21}. If the laser counter-propagates with the electron beam, however, it leads to an enhancement as $\eta \simeq 2\gamma E_\perp / E_{Sch}$, which can lower the threshold of QED cascade from vacuum²⁷ and has been extensively discussed in the context of γ -ray explosion^{28,29} and pair plasma generation³⁰⁻³³.

In order to exploit the counter-propagating configuration, in this Letter, a CP femtosecond pulse was irradiated on a compound target (in Fig.1) consisting of a near-critical-density (NCD) plasma slab and a solid foil. Here the overdense foil is used to reflect the driven light spontaneously as a plasma mirror³⁴. Generally, when a CP pulse of 10^{19-21} W/cm² propagates in the NCD plasma, the radial electrostatic field $\mathbf{E}_{Sr} = k_E r \hat{e}_r$ and quasistatic azimuthal magnetic field $\mathbf{B}_{S\theta} = -k_B r \hat{e}_\theta$ are generated in the excavated plasma channel^{35,36}. A collimated energetic electron beam with overcritical density and helical structure can be achieved in resonant regime³⁷⁻³⁹ when electron betatron frequency $\omega_\beta = \sqrt{e(v_\parallel k_B + k_E)/(\gamma m_e)}$ is close to the light frequency witnessed by the electron $\omega_L = (1 - v_\parallel/v_{ph})\omega_0$. Here v_{ph} is the phase velocity of light in plasma and ω_0 is the light frequency in laboratory frame. Under the higher intensity of $\sim 10^{23}$ W/cm², however, electrons are mostly expelled from the high-intensity region and a hollow channel is merely filled with laser radiation⁴⁰. More interestingly, a great amount of electrons will be trapped back into the channel if radiation reaction (RR) is taken into account^{40,41}, where transverse ponderomotive force is properly balanced by the radiation recoil.

To understand the underlying mechanism of RR influence in the scheme, the evolution of the relative phase ψ between the electron rotation and the periodic laser field was explored. Based on previous work^{36,38,42}, the time derivative of the ponderomotive phase ψ can be written as

$$\frac{d\psi}{dt} = \omega_\beta - \omega_l = \sqrt{\frac{e}{\gamma m_e}(v_\parallel k_B + k_E)} - (1 - v_\parallel/v_{ph})\omega_0. \quad (1)$$

The time derivative of the electron Lorentz factor is

$$\frac{d\gamma}{dt} = -\frac{\mathbf{v} \cdot (e\mathbf{E} + \mathbf{f}_{rad})}{m_e c^2} = -\frac{ev_\perp E_L \cos\psi}{m_e c^2} - \epsilon_{rad} \omega_0 \beta^2 a_s^2 \eta^2 G(\eta). \quad (2)$$

Here E_L is the light electromagnetic field. RR force $\mathbf{f}_{rad} \approx -G(\eta)\epsilon_{rad}m_e c \omega_0 \vec{\beta} a_s^2 \eta^2$ for ultrarelativistic limit $\gamma \gg 1$ is included, where $G(\eta)$ corresponds to radiation weaken correction induced by nonlinear QED effect⁴³. $\epsilon_{rad} = 4\pi r_e/3\lambda_0$, $r_e = e^2/m_e c^2$ is the electron radius and λ_0 is the laser wavelength. $\vec{\beta} = \vec{v}/c$ is the normalized velocity and $a_s = eE_{Sch}/m_e \omega_0 c$ is the normalized Schwinger field. From Eqs.(1)-(2), it can be found that the phase space (ψ, γ) has a fixed point at $(\psi_0, \gamma_0) = (\arccos \frac{-\epsilon_{rad} \omega_0 \beta^2 a_s^2 \eta^2 G(\eta) m_e c^2}{ev_\perp E_L}, \frac{e(v_\parallel k_B + k_E)}{m_e(1 - v_\parallel/v_{ph})^2 \omega_0^2})$. To determine the system dynamic property from Eqs.(1)-(2) in (ψ, γ) space, the perturbation expansion nearby (ψ_0, γ_0) of Eqs.(1)-(2) was made and quadratic terms were dropped to arrive at the characteristic Jacobian matrix \mathbf{J}_a ^{44,45}:

$$\mathbf{J}_a \approx \begin{pmatrix} 0 & -\frac{1}{2} \sqrt{\frac{e}{\gamma^3 m_e}(v_\parallel k_B + k_E)} \\ ev_\perp E_L \sin\psi & -\epsilon_{rad} m_e c^2 \omega_0 \beta^2 a_s^2 \frac{\partial G(\eta) \eta^2}{\partial \gamma} \end{pmatrix}_{\psi_0, \gamma_0} \quad (3)$$

Without RR, the trace and determinant of Jacobian matrix are $\text{tr}(\mathbf{J}_a) = 0$ and $\text{det}(\mathbf{J}_a) > 0$, which manifests that (ψ_0, γ_0) is a center without any source or sink property^{44,45}. On the contrary, with RR effect being considered, at fixed point $\text{tr}(\mathbf{J}_a) < 0$ and $\text{det}(\mathbf{J}_a) > 0$ indicates that its behaviour converts from center to spiral sink attractor⁴⁶. The sink attractor emerging illustrates a large fraction of the radiation trapped electrons tends to possess the relative phase ψ_0 with respect to laser electric field and the helical density structure is an intrinsic rotary manner of the electric field of CP laser. It should be noted that for electron moving in the same direction as the pulse, the magnetic field of the laser pulse counteracts the force from the laser electric field leading to $\eta \sim 0$ and $\text{tr}(\mathbf{J}_a) \sim 0$. However, the strong self-generated magnetic field $B_{s\theta} \approx \mu_0 n_e c R/2$ (here μ_0 is the permeability of free space, n_e is the RR trapped electron density and R is the channel radius) approaching the order of driven laser field²⁵ gives $\eta \approx \frac{\gamma B_{s\theta}}{E_{Sch}}$, which results in $\text{tr}(\mathbf{J}_a) \approx -2\epsilon_{rad} \beta^2 e^2 B_{s\theta}^2 / m_e \omega_0 < 0$ and enables the attractor influence on achieving such a helical electron bunch (HEB). The total OAM acquired by the HEB can be calculated as

$$L \approx - \int \Sigma_i e r_\perp E_L \cos\psi_i dt \quad i = 1, 2, 3... \quad (4)$$

here r_\perp is the electron transverse radius and the index i refers to each electron. From Eq.(4) we can see that the laser could transfer its spin angular momentum (SAM) to HEB only when most of electrons possess the same relative phase ψ_i , otherwise ensemble average leads to $\Sigma_i \cos\psi_i \approx 0$. Therefore, coupling effects among RR trapping, self-generated magnetic field and spiral attractor in phase space, play key roles in realizing the HEB and net OAM gain. Eventually nonlinear QED effect⁴⁷ enhances the discrete quantum emission^{48,49} in the inverse Compton scattering (ICS) between HEB and the reflected light, where prolific gamma photons inheriting a large fraction of electrons' OAM are generated. Here we demonstrate the validity and the robustness of this scheme by using the self-consistent three dimension PIC code EPOCH⁵⁰ (see Methods).

PIC simulation results

The electron density distributions in $\gamma - \psi$ space at $t=50T_0$ for the cases with and without RR are presented in Figs.2(a) and (b). When RR force is switched on, most of electrons possess a relative phase $\psi=2.3$ (in Fig.2(b)) which is in good agreement with our theoretically derived attractor point $(\psi_0, \gamma_0)=(2.24, 3416)$ (see Methods). Since neither RR trapping nor attractor emerging occurs, the number of electron in Fig.2(a) is relatively small compared to RR case and it does not behave concentration like the attractor modulated distribution. The self-generated azimuthal magnetic field $B_{s\theta}$ averaged over the channel in the cross $z=0$ is plotted in Fig.2(c) with maximum $\approx 0.6\text{MT}$ (normalized value equals $60m_e\omega/e \approx 0.2B_L$, where B_L is the laser magnetic amplitude) at $t=65T_0$, which demonstrates that RR recoil has promotion on $B_{s\theta}$ generation due to the more trapped electron current along the longitudinal axis. The temporal evolution of electron number inside the plasma channel and their total OAM $L = \sum_i r_i \times p_i = \sum_i y_i p_{zi} - z_i p_{yi}$ are recorded in Fig.2(d) for both cases, from which it is found that RR not only boosts the electron accumulation inside the channel but also facilitates the OAM transfer to HEB, which is in good agreement with the theoretical prediction of Eq.(4). The RR force prevents electrons from being expelled transversely, resulting in a increase of electrons from 172 nano-Coulombs(nC) to 291 nC at $t=65T_0$. The enhancement of electron current strengthens the $B_{s\theta}$, which gives a positive feedback on spiral attractor merging in phase space and effectively favours angular momentum transformation from laser's SAM to HEB's OAM.

Since the ponderomotive force of CP pulse avoids the longitudinal oscillation at twice the optical frequency⁵¹, plasma in the second layer cannot be heated efficiently and the driven light is substantially reflected. Under colliding configuration, the parameter $\eta \approx 2\gamma E_L/E_{Sch} \gtrsim 1$ indicates that the discrete incoherent photon emission²¹ gives a more appropriate description compared with the coherent electromagnetic wave radiation derived from the Liénard-Wiechert retarded potential⁵². The volume snapshot of the photon energy density at $t=70T_0$ is exhibited in Fig.3(a) where photon beam inherits spatial helical structure and transverse size of the source is about $1.5\mu\text{m}$. The gamma-ray flash duration is $\sim 16\text{fs}$ roughly equal to half of the laser duration because the driven pulse and trapped electrons completely overlap inside the channel. The angular-spectral distribution calculated by accumulating the forward photons at $t=70T_0$ over the entire simulation region is shown in Figs.3(b) and (c). Most of energetic photons are highly collimated and predominantly located within an emission polar angle $\phi \leq 15^\circ$ ($\phi \leq 30^\circ$) for energies higher than 1GeV (100MeV). In a 0.1% bandwidth (BW) around 1GeV we have 1.05×10^8 photons, implying the brightness of 1.7×10^{23} photons/s/mm²/mrad²/0.1%BW for the GeV gamma-ray emission. The corresponding source brilliances at 100 MeV and 10 MeV are 2.3×10^{24} and 1.5×10^{25} photons/s/mm²/mrad²/0.1%BW, respectively.

In Fig.4(a), the exponential decay spectrum of photon covers higher energy range from 1MeV to several GeV with a cutoff energy at 2.9GeV and that of the electron before($t=60T_0$) and after($t=70T_0$) ICS process are also presented. The characteristic kinetic energy for the electron nearby the spiral attractor point (γ_0, ψ_0) is expressed as $\gamma_0 = (v_{\parallel}/c) \cdot (n_e/n_c) / [2 - 2(v_{\parallel}/c) \sqrt{1 - n_e/(n_c a_0)}]^2 m_e c^2 \approx 1.7\text{GeV}$, here the estimated $v_{\parallel}=0.9863c$, $n_e=2n_c$ and $a_0=300$ corresponding to simulation parameters. The nonlinear QED regime predicts that most photons are emitted with an energy $h\nu_{ph} \approx 0.44\eta\gamma m_e c^2$ ^{230,43} which carries a large fraction of electron's kinetic energy. It is obvious that the amount of high-energy electron is drastically curtailed with the cutoff-energy declining from 3.9GeV to 2.5GeV and simultaneously most of energy is converted to gamma photons. The temporal evolutions of the particle energy are illustrated in Fig.4(b), where 14.5%/4.2%/0.108% of the total laser energy is transferred into the gamma-ray photon with energy above 1MeV/100MeV/1GeV. For energies above 100MeV/1GeV, the photons are emitted almost exclusively by ICS process during $65T_0 < t < 70T_0$ as shown in Fig.4(b). Based on power radiated by a single electron, $P_{rad} \propto \eta$ ^{253,54}, the instantaneous radiation power of this regime can be estimated as

$$P_{rad} = \begin{cases} N_e \frac{4\pi\alpha_f m_e c^3}{3\lambda_c} \left(\frac{\gamma B_{s\theta}}{E_{Sch}}\right)^2 G\left(\frac{\gamma B_{s\theta}}{E_{Sch}}\right) & t < t_{ref} \\ N_e \frac{4\pi\alpha_f m_e c^3}{3\lambda_c} \left(\frac{2\gamma E_l}{E_{Sch}}\right)^2 G\left(\frac{2\gamma E_l}{E_{Sch}}\right) & t \geq t_{ref} \end{cases} \quad (5)$$

here $\lambda_c = h/m_e c$ is the Compton wavelength and $t_{ref}=65T_0$ is the moment of light reflecting. Eq.(5) predicts the radiation power $P_{rad} \approx 0.63\text{PW}$ ($t < t_{ref}$) and $P_{rad} \approx 19.2\text{PW}$ ($t \geq t_{ref}$), implying the nonlinear QED ICS based gamma-ray source power of the same order as the infrared incident laser.

The transfer of OAM in longitudinal direction from the laser to the particles is plotted in Fig.4(c). In terms of quantum mechanics, the angular momentum carried by a photon of CP laser is $\sigma = \pm 1$ for spin motion. The total angular momentum absorbed from laser is approximately expressed as $L_l = \delta \frac{W_l}{\hbar\omega_{laser}} \sigma \hbar = 1.70 \times 10^{-12} \delta \text{ kg}\cdot\text{m}^2/\text{s}$, where W_l is the whole laser energy and δ is the absorbing ratio. During ICS process, OAM is more efficiently transferred from electron to gamma-ray and eventually the OAM of photons reaches $8.2 \times 10^{-14} \text{ kg}\cdot\text{m}^2/\text{s}$, 4.8% of the total laser SAM. In addition, a parameter scan has been carried out to investigate energy conversion efficiency for a wide range (0.2-20 n_c) of initial first layer plasma density in Fig.4(d) and find that there is an optimal condition $n_e \sim n_c$ for realizing the twisted GeV gamma-ray emission. The disadvantage for relatively rarefied plasma ($n_e=0.2n_c$) is lack in trapped helical electron amount so that insufficient electron quantity accounts

for deficient gamma-ray production, while for relatively dense circumstance ($n_e \gtrsim 10n_c$) driven laser tends to deplete most of their energy in the first slab and without any remnants to trigger ICS process.

Discussion

To conclude, we have shown how the ultra-intense and ultra-bright GeV twisted gamma-ray flash can be achieved by irradiating a prospective $1.2 \times 10^{23} \text{ W/cm}^2$ laser on a compound plasma target in nonlinear QED regime. The initial energetic HEB results from the coupling effects among RR trapping, self-generated magnetic field and emergency of spiral attractor in γ - ψ space. The twisted gamma-ray flash inherits a considerable OAM and energy of the parent electron beam through Compton backscattering between HEB and the reflected driven pulse. The final photon source, with unprecedented power of 20 PW and brightness of $1.7 \times 10^{23} \text{ photons/s/mm}^2/\text{mrad}^2/0.1\%$ (at 1 GeV), might enable significant development of application in particles physics⁵⁵ and laboratory astrophysics¹⁵. Our scheme is also feasible in the laboratory system where cluster jets⁵⁶ or nano-tube foams⁵⁷ can be utilized for NCD plasma generation and a solid foil acts as a plasma mirror to reflect laser³⁴. Such parameters of the gamma-ray sources will be achieved with a next generation of multi-PW laser facilities in the future.

Methods

Set-up of numerical simulations and simulation parameters. Simulations have been performed using the fully relativistic, electro-magnetic PIC code Epoch⁵⁰. A Monte Carlo probabilistic approach^{53,54} has been successfully implemented, which is based on QED corrected synchrotron cross sections and coupled with the subsequent reduction of the electron momentum. Each particle is assigned an optical depth at which it emits (τ) according to $P = 1 - e^{-\tau}$, where $P \in [0,1]$ is chosen at random to consider the quantum correction in the emission processes as well as the straggling. The rates of photon production, $d\tau_\gamma/dt = (\sqrt{3}\alpha_f c \eta)/(\lambda_c \gamma) \int_0^{\eta/2} d\chi F(\eta, \chi)/\chi$, are then solved until the optical depth is reached, when the emission event occurs⁵³. Here, $\chi = (\hbar\omega_{ph}/2m_e c^2)|\mathbf{E}_\perp + \hat{\mathbf{k}} \times c\mathbf{B}|/E_{Sch}$, where the subscript \perp denotes the component perpendicular to the unit vector in the photon's direction of motion $\hat{\mathbf{k}}$ and $\hbar\omega_{ph}$ is the photon energy.

The incident $1.2 \times 10^{23} \text{ W/cm}^2$ CP pulse propagates along X direction with a profile of $a = a_0 e^{-(t-t_0)^4/\tau_0^4} e^{-(y^2+z^2)/r_0^2} \sin(\omega_0 t)$, where $a_0 = eE_L/m_e \omega_0 c = 300$ is the normalized amplitude of the laser field. $t_0 = 6T_0$ and $\tau_0 = 5T_0$ denotes the pulse with a temporal duration of $12T_0$ ($T_0 \approx 3.3\text{fs}$ is the laser period). $r_0 = 5\lambda_0$ is the spot size ($\lambda_0 = 1.0\mu\text{m}$). The simulation box is $80\lambda_0 \times 40\lambda_0 \times 40\lambda_0$ in X \times Y \times Z direction, which has been divided into $3200 \times 800 \times 800$ cells. A hydrogen slab with initial density of $n_e = 2n_c$ locates between $10\lambda_0$ to $60\lambda_0$ and aluminum foil of $n_e = 700n_c$ is placed from $60\lambda_0$ to $80\lambda_0$, where $n_c = m_e \omega_0^2/4\pi e^2$ is critical density⁵¹. The hydrogen slab and aluminum foil contain 4 and 16 macroparticles per cell (for both species), respectively. For reference, there is no influence on our conclusions and results when we double the number of macroparticle per cell.

Calculation of attractor in phase space. Lorentz factor at fixed point obtained from Eqs.(1)-(2) as $\gamma_0 = \frac{e(v_{\parallel} k_B + k_E)}{m_e(1-v_{\parallel}/v_{ph})^2 \omega_0^2} \approx \frac{(v_{\parallel}/c)(n_e/n_c)}{2[1-v_{\parallel}/c\sqrt{1-n_e/(a_0 n_c)}]^2}$ where $k_B \approx \frac{en_e}{2\epsilon_0}$, $\omega_0 = \sqrt{\frac{n_c e^2}{\epsilon_0 m_e}}$ and $v_{ph} \approx \frac{c}{\sqrt{1-n_e/(a_0 n_c)}}$ are taken into account and the k_E as the transverse static electric field is neglected as it is relatively weak compared with self-generated magnetic field. Substituting $n_e = 2n_c$, $a_0 = 300$ and $v_{\parallel} = 0.9863c$ (from simulation parameters and results) into above equation leads to $\gamma_0 = 3416$. Considering $\epsilon_{rad} = 1.18 \times 10^{-8} (\frac{1\mu\text{m}}{\lambda_0})$, $\beta \approx 1$, $a_s \approx 3.8 \times 10^5$, $\eta \approx \frac{\gamma_0 B_{s0}}{a_s} \approx 0.178$, $G(\eta) \approx 1$ and $v_{\perp} = 0.165c$, the relative phase is deduced as $\psi_0 = \arccos \frac{-\epsilon_{rad} \omega_0 \beta^2 a_s^2 \eta^2 G(\eta) m_e c^2}{e v_{\perp} E_L} \approx 2.24$.

References

1. Allen, L., Beijersbergen, M. W., Spreeuw, R. & Woerdman, J. Orbital angular momentum of light and the transformation of laguerre-gaussian laser modes. *Phys. Rev. A* **45**, 8185 (1992).
2. Padgett, M. & Bowman, R. Tweezers with a twist. *Nat. Photonics* **5**, 343–348 (2011).
3. Wang, J. *et al.* Terabit free-space data transmission employing orbital angular momentum multiplexing. *Nat. Photonics* **6**, 488–496 (2012).
4. Bozinovic, N. *et al.* Terabit-scale orbital angular momentum mode division multiplexing in fibers. *Sci.* **340**, 1545–1548 (2013).
5. Mair, A., Vaziri, A., Weihs, G. & Zeilinger, A. Entanglement of the orbital angular momentum states of photons. *Nat.* **412**, 313–316 (2001).
6. Molina-Terriza, G., Torres, J. P. & Torner, L. Twisted photons. *Nat. Phys.* **3**, 305–310 (2007).

7. Beijersbergen, M., Coerwinkel, R., Kristensen, M. & Woerdman, J. Helical-wavefront laser beams produced with a spiral phaseplate. *Opt. Commun.* **112**, 321–327 (1994).
8. Basistiy, I., Soskin, M. & Vasnetsov, M. Optical wavefront dislocations and their properties. *Opt. Commun.* **119**, 604–612 (1995).
9. Gariepy, G. *et al.* Creating high-harmonic beams with controlled orbital angular momentum. *Phys. review letters* **113**, 153901 (2014).
10. Hemsing, E. & Marinelli, A. Echo-enabled x-ray vortex generation. *Phys. review letters* **109**, 224801 (2012).
11. Hemsing, E. *et al.* Coherent optical vortices from relativistic electron beams. *Nat. Phys.* **9**, 549–553 (2013).
12. Petrillo, V., Dattoli, G., Drebot, I. & Nguyen, F. Compton scattered x-gamma rays with orbital momentum. *Phys. Rev. Lett.* **117**, 123903 (2016).
13. Ivanov, I. P. Colliding particles carrying nonzero orbital angular momentum. *Phys. Rev. D* **83**, 093001 (2011).
14. Torner, L., Torres, J. P. & Carrasco, S. Digital spiral imaging. *Opt. Express* **13**, 873–881 (2005).
15. Tamburini, F., Thidé, B., Molina-Terriza, G. & Anzolin, G. Twisting of light around rotating black holes. *Nat. Phys.* **7**, 195–197 (2011).
16. Extreme light infrastructure project. www.eli-laser.eu.
17. Exawatt center forextreme light studies. www.xcels.iapras.ru.
18. Bulanov, S. *et al.* On the design of experiments for the study of extreme field limits in the interaction of laser with ultrarelativistic electron beam. *Nucl. Instruments Methods Phys. Res. Sect. A: Accel. Spectrometers, Detect. Assoc. Equip.* **660**, 31–42 (2011).
19. Bulanov, S. *et al.* On the problems of relativistic laboratory astrophysics and fundamental physics with super powerful lasers. *Plasma Phys. Reports* **41**, 1–51 (2015).
20. Di Piazza, A., Hatsagortsyan, K. & Keitel, C. H. Quantum radiation reaction effects in multiphoton compton scattering. *Phys. review letters* **105**, 220403 (2010).
21. Di Piazza, A., Müller, C., Hatsagortsyan, K. & Keitel, C. Extremely high-intensity laser interactions with fundamental quantum systems. *Rev. Mod. Phys.* **84**, 1177 (2012).
22. Ridgers, C. *et al.* Dense electron-positron plasmas and ultraintense γ rays from laser-irradiated solids. *Phys. review letters* **108**, 165006 (2012).
23. Brady, C. S., Ridgers, C., Arber, T., Bell, A. & Kirk, J. Laser absorption in relativistically underdense plasmas by synchrotron radiation. *Phys. review letters* **109**, 245006 (2012).
24. Nakamura, T. *et al.* High-power γ -ray flash generation in ultraintense laser-plasma interactions. *Phys. review letters* **108**, 195001 (2012).
25. Stark, D., Toncian, T. & Arefiev, A. Enhanced multi-mev photon emission by a laser-driven electron beam in a self-generated magnetic field. *Phys. review letters* **116**, 185003 (2016).
26. Schwinger, J. On gauge invariance and vacuum polarization. *Phys. Rev.* **82**, 664 (1951).
27. Bulanov, S. S., Mur, V. D., Narozhny, N. B., Nees, J. & Popov, V. S. Multiple colliding electromagnetic pulses: A way to lower the threshold of e^+e^- pair production from vacuum. *Phys. Rev. Lett.* **104**, 220404 (2010).
28. Nerush, E. *et al.* Laser field absorption in self-generated electron-positron pair plasma. *Phys. review letters* **106**, 035001 (2011).
29. Gong, Z. *et al.* High-efficiency γ -ray flash generation via multiple-laser scattering in ponderomotive potential well. *Phys. Rev. E* **95**, 013210 (2017).
30. Bell, A. & Kirk, J. G. Possibility of prolific pair production with high-power lasers. *Phys. review letters* **101**, 200403 (2008).
31. Zhu, X.-L. *et al.* Dense gev electron-positron pairs generated by lasers in near-critical-density plasmas. *Nat. Commun.* **7**, 13686 (2016).
32. Jirka, M. *et al.* Electron dynamics and γ and e^-e^+ production by colliding laser pulses. *Phys. Rev. E* **93**, 023207 (2016).
33. Chang, H. *et al.* Generation of overdense and high-energy electron-positron-pair plasmas by irradiation of a thin foil with two ultraintense lasers. *Phys. Rev. E* **92**, 053107 (2015).

34. Phuoc, K. T. *et al.* All-optical Compton gamma-ray source. *Nat. Photonics* **6**, 308–311 (2012).
35. Pukhov, A., Sheng, Z.-M. & Meyer-ter Vehn, J. Particle acceleration in relativistic laser channels. *Phys. Plasmas (1994-present)* **6**, 2847–2854 (1999).
36. Pukhov, A. Strong field interaction of laser radiation. *Reports on progress Phys.* **66**, 47 (2002).
37. Liu, B. *et al.* Generating overcritical dense relativistic electron beams via self-matching resonance acceleration. *Phys. review letters* **110**, 045002 (2013).
38. Hu, R. *et al.* Dense helical electron bunch generation in near-critical density plasmas with ultrarelativistic laser intensities. *Sci. reports* **5** (2015).
39. Arefiev, A. V., Breizman, B. N., Schollmeier, M. & Khudik, V. N. Parametric amplification of laser-driven electron acceleration in underdense plasma. *Phys. review letters* **108**, 145004 (2012).
40. Ji, L., Pukhov, A., Kostyukov, I. Y., Shen, B. & Akli, K. Radiation-reaction trapping of electrons in extreme laser fields. *Phys. review letters* **112**, 145003 (2014).
41. Chang, H. *et al.* Brilliant petawatt gamma-ray pulse generation in quantum electrodynamic laser-plasma interaction. (*unpublished*) (2016).
42. Liu, B. *et al.* Quasimonoeenergetic electron beam and brilliant gamma-ray radiation generated from near critical density plasma due to relativistic resonant phase locking. *Phys. Plasmas (1994-present)* **22**, 080704 (2015).
43. Kirk, J. G., Bell, A. & Arka, I. Pair production in counter-propagating laser beams. *Plasma Phys. Control. Fusion* **51**, 085008 (2009).
44. Jordan, D. & Smith, P. *Nonlinear ordinary differential equations: an introduction for scientists and engineers* (Oxford University Press on Demand, 2007).
45. Hirsch, M. W., Smale, S. & Devaney, R. L. *Differential equations, dynamical systems, and an introduction to chaos* (Academic press, 2012).
46. Gong, Z. *et al.* Radiation reaction induced spiral attractors in ultra-intense colliding laser beams. *Matter Radiat. at Extrem.* (2016).
47. Ritus, V. Quantum effects of the interaction of elementary particles with an intense electromagnetic field. *J. Russ. Laser Res.* **6**, 497–617 (1985).
48. Neitz, N. & Di Piazza, A. Stochasticity effects in quantum radiation reaction. *Phys. review letters* **111**, 054802 (2013).
49. Blackburn, T., Ridgers, C., Kirk, J. G. & Bell, A. Quantum radiation reaction in laser–electron-beam collisions. *Phys. review letters* **112**, 015001 (2014).
50. Arber, T. *et al.* Contemporary particle-in-cell approach to laser-plasma modelling. *Plasma Phys. Control. Fusion* **57**, 113001 (2015).
51. Gibbon, P. *Short pulse laser interactions with matter* (World Scientific Publishing Company, 2004).
52. Jackson, J. D. *Classical electrodynamics* (Wiley, 1999).
53. Duclous, R., Kirk, J. G. & Bell, A. Monte Carlo calculations of pair production in high-intensity laser–plasma interactions. *Plasma Phys. Control. Fusion* **53**, 015009 (2010).
54. Ridgers, C. *et al.* Modelling gamma-ray photon emission and pair production in high-intensity laser–matter interactions. *J. Comput. Phys.* **260**, 273–285 (2014).
55. Pike, O., Mackenroth, F., Hill, E. & Rose, S. A photon-photon collider in a vacuum hohlraum. *Nat. Photonics* **8**, 434–436 (2014).
56. Fukuda, Y. *et al.* Energy increase in multi-MeV ion acceleration in the interaction of a short pulse laser with a cluster-gas target. *Phys. review letters* **103**, 165002 (2009).
57. Ma, W. *et al.* Directly synthesized strong, highly conducting, transparent single-walled carbon nanotube films. *Nano Lett.* **7**, 2307–2311 (2007).

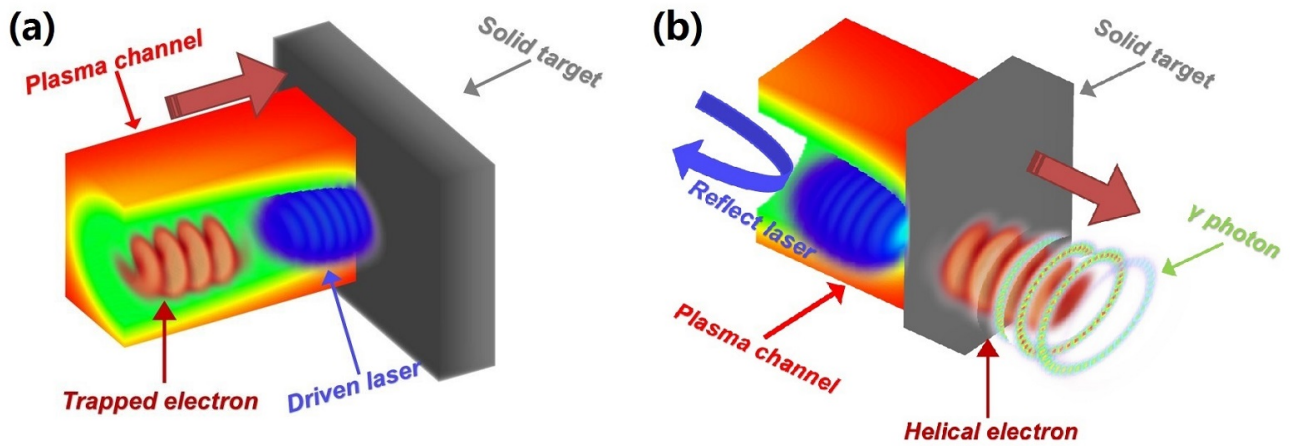


Figure 1. Schematic diagram of the OAM gamma-ray source. (a) and (b) show light being reflected before and after respectively.

Acknowledgements

The work has been supported by the National Basic Research Program of China (Grant No.2013CBA01502), NSFC (Grant Nos.11535001 and 11575011) and National Grand Instrument Project (2012YQ030142). The PIC code Epoch was in part funded by the UK EPSRC grants EP/G054950/1, EP/G056803/1, EP/G055165/1 and EP/M022463/1. J.Q. Yu wants to thank the Project 2016M600007 funded by China Postdoctoral Science Foundation. Our simulations were carried out in Max Planck Computing and Data Facility and Shanghai Super Computation Center. The author Z.Gong acknowledges fruitful discussions with S.V. Bulanov and H.X. Chang.

Author contributions statement

H.L., X.Y, C.C. and X.H. conducted the work. Z.G., R.H. and J.Y. developed the basic theory. Z.G. carried out all simulations. Some details of the physics are clarified by R.H., H.L. and X.Y. The manuscript is written by Z.G. and R.H. All authors reviewed this manuscript.

Additional information

Competing financial interests:(The authors declare no competing financial interests).

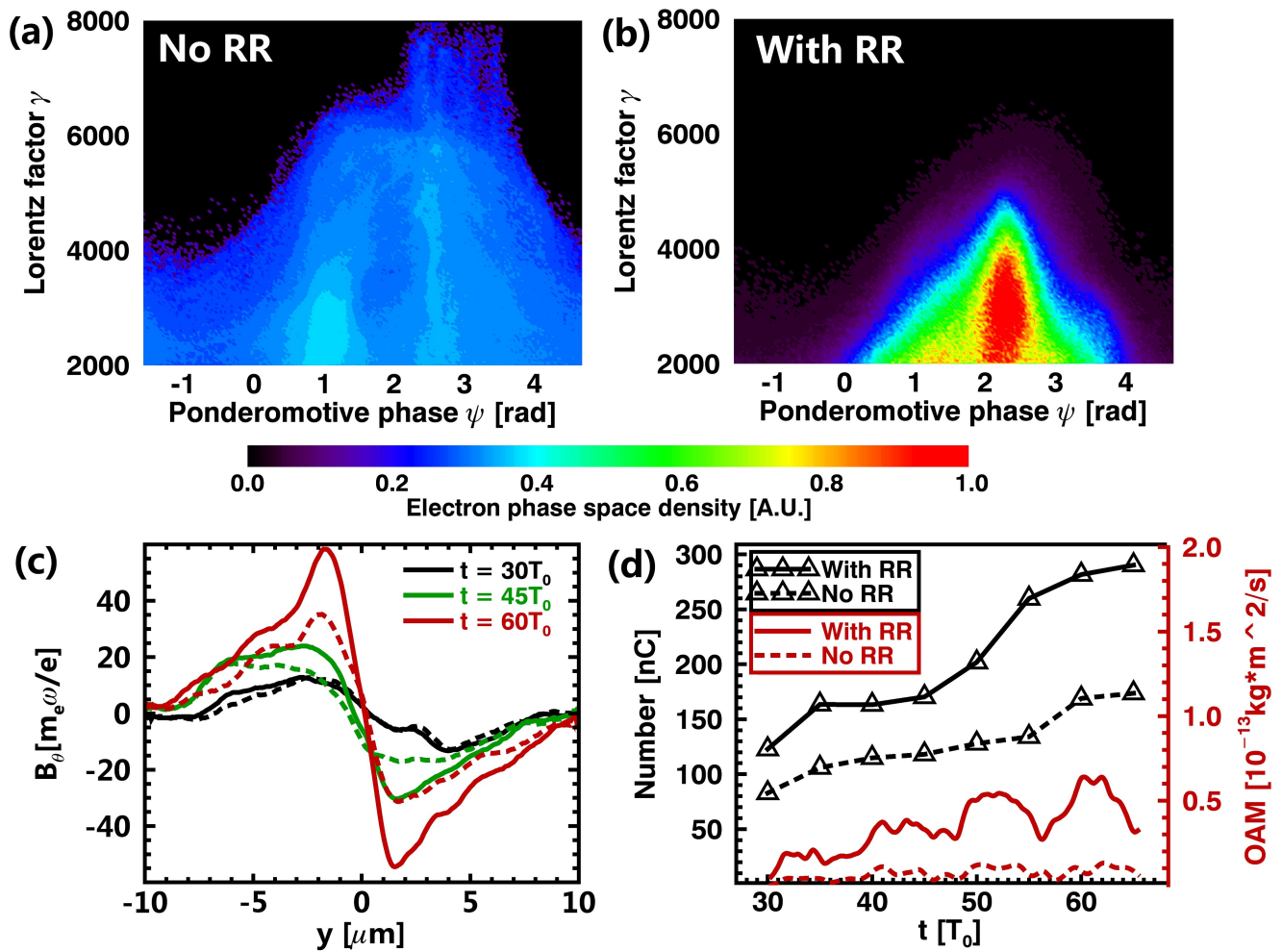


Figure 2. Distribution of electron density in ψ - γ space at $t=50T_0$ with RR (a) and without RR (b), respectively. (c) Normalized amplitude of $B_{s\theta}$ averaged over the channel in the plane $z=0$ at time $t=30, 45, 60 T_0$, where solid/dash line corresponds to the with/without RR circumstance. (d) presents the number of the electron inside the channel and total OAM of electrons in x direction as a function of the interaction time t , where solid (dash) denotes the with (without) RR case.

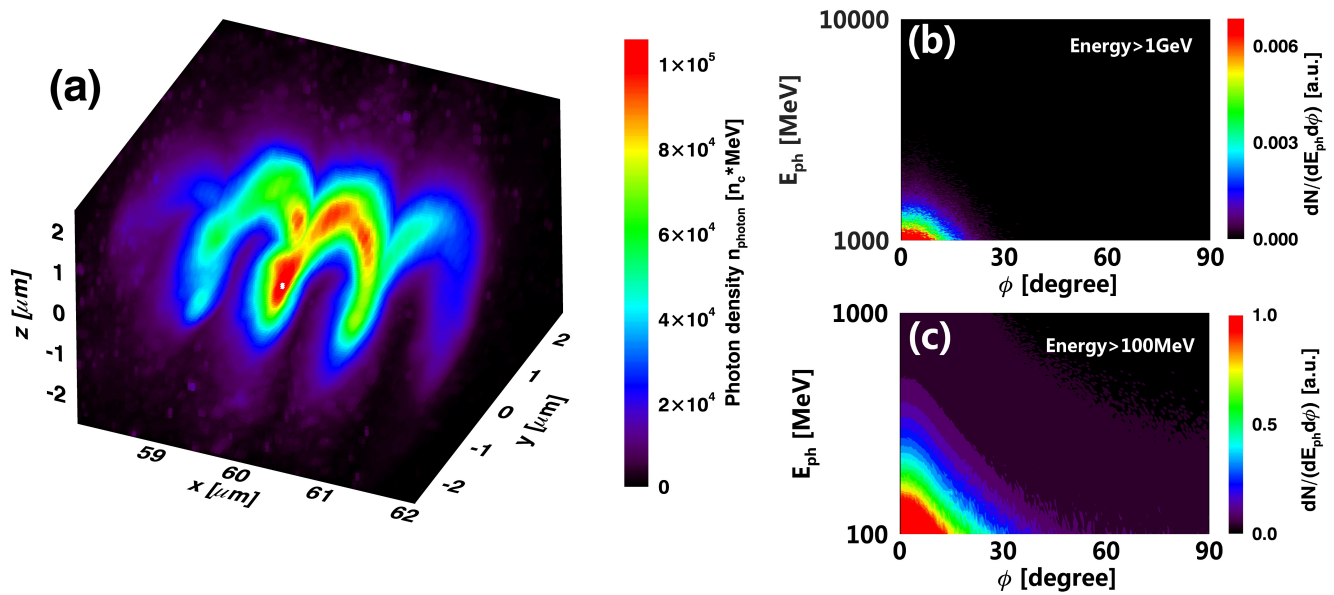


Figure 3. (a) Volume distribution of the photon energy density where only photon with energy higher than 10MeV is recorded from the viewpoint of computation costs. (b)(c) Final photon angular-spectral distribution for energy higher than 1GeV and 100MeV respectively, where ϕ is defined as $\phi = \arctan \frac{v_{\perp}}{v_{\parallel}}$.

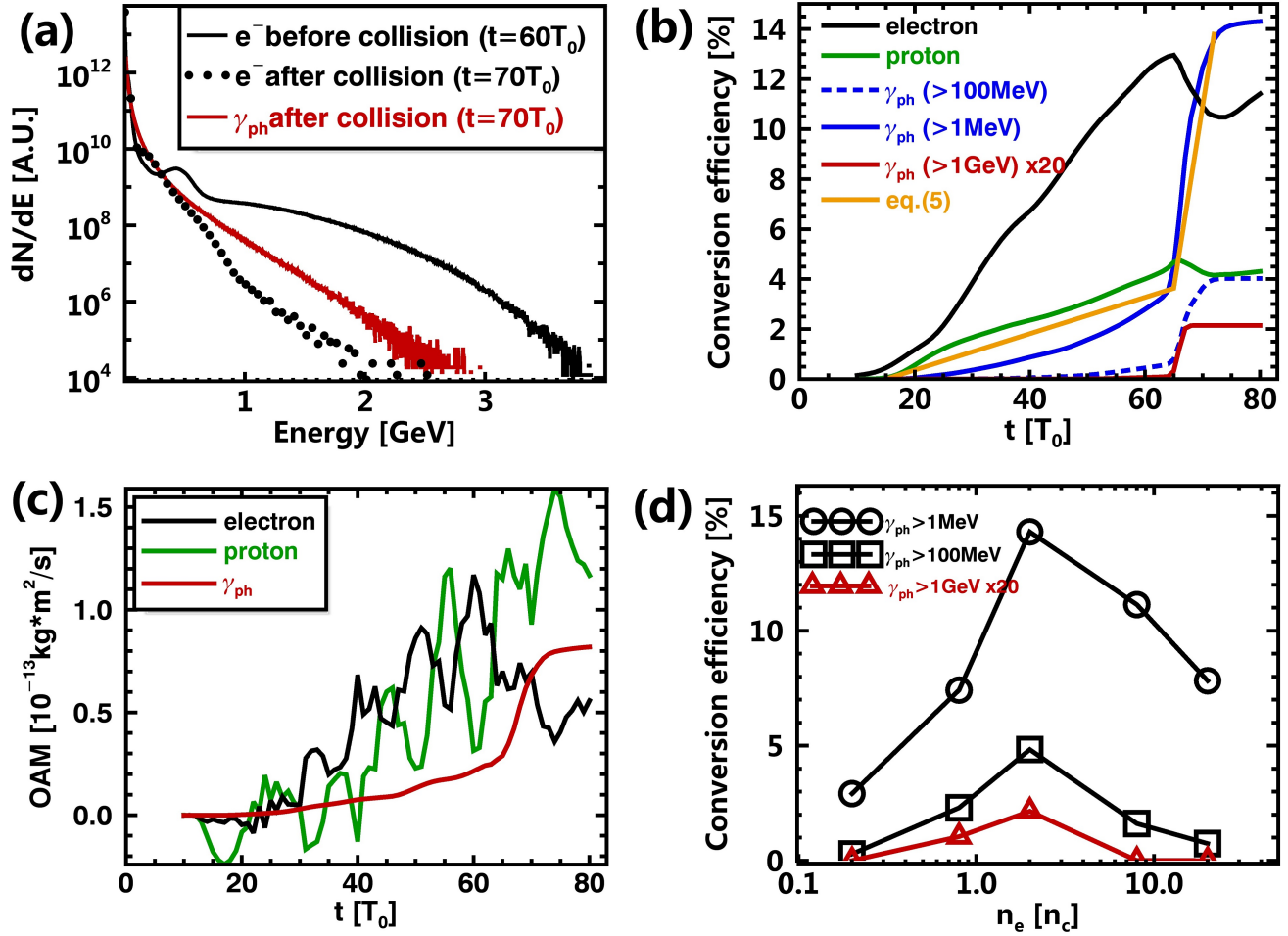


Figure 4. (a) The energy spectra of electrons at $t=60,70T_0$ and photons at $t=70T_0$. (b) The laser energy conversion to the electrons (black), protons (green) and gamma-ray photons ($>1\text{MeV}$ in solid blue, $>100\text{MeV}$ in dash blue and $>1\text{GeV}$ in solid red where the value of $>1\text{GeV}$ times by 20 is exhibited). The orange solid line plots the radiation power prediction from eq.(5). (c) Temporal evolution of the total OAM of electrons, protons and photons. (d) The energy conversion efficiency from laser to γ -photons with different plasma densities. Here the value of $\gamma_{ph} > 1\text{GeV}$ is times by 20 and the horizontal (density) axis is on a logarithmic scale.